frontiers | Frontiers in Earth Science

TYPE Original Research
PUBLISHED 13 March 2024
DOI 10.3389/feart.2024.1371358

OPEN ACCESS

EDITED BY
Xixin Wang,
Yangtze University, China

REVIEWED BY
Lei Gong,
Northeast Petroleum University, China
Yu Liu,
China University of Mining and Technology, Beijing, China

*CORRESPONDENCE
Xiaodong Lan,
lansecup@163.com

RECEIVED 16 January 2024
ACCEPTED 15 February 2024
PUBLISHED 13 March 2024

CITATION
Lan X, Bai Z, Yang Y, Jiang Z and Zhang J (2024), Source and geological significance of Jurassic asphalt in the Ruoqiang Sag of Southeast Depression, Tarim Basin, Northwestern China.
Front. Earth Sci. 12:1371358.
doi: 10.3389/feart.2024.1371358

Source and geological significance of Jurassic asphalt in the Ruoqiang Sag of Southeast Depression, Tarim Basin, Northwestern China

Xiaodong Lan[1]*, Zhongkai Bai[2], Youxing Yang[2], Zhenglong Jiang[1] and Jile Zhang[1]

[1]School of Ocean Sciences, China University of Geosciences, Beijing, China, [2]Oil and Gas Survey, China Geological Survey, Beijing, China

The Southeast Depression of the Tarim Basin has a very low petroleum exploration degree, and currently, no industrial oil and gas have been discovered. Many hydrocarbon shows exist in the Ruoqiang Sag, where hydrocarbon sources and accumulation processes are unclear. Only two potential Jurassic hydrocarbon source rocks developed in the Ruoqiang Sag, the Yangye (J_2y) lacustrine mudstone of the Middle Jurassic and the Kangsu (J_1k) coal-bearing mudstone of the Lower Jurassic. In this study, the Jurassic asphalt found in the QD1 well, combined with the source rocks of drilling cores and outcrops, was used to explore the possible hydrocarbon source and forming process in the Ruoqiang Sag using oil-source correlation and hydrocarbon accumulation geochronology methods. The asphalts have lower light and heavy rare earth fractionation than the J_2y mudstone, and the total rare earth element (ΣREE) content, chondrite-normalized curves, and δEu and Y/Ho values are similar to those of the J_1k mudstone, especially for the J_1k coal. The *n*-alkane ratios of the carbon preference index and the odd-to-even preference (OEP) of Jurassic asphalts are greater than 1.0, indicating that its source rock has experienced low thermal evolution. All Jurassic samples have similar source-related biomarkers but different maturity-related parameters, and the thermal evolution degree of asphalt is close to the J_1k mudstone and coal but slightly higher than the J_2y mudstone. Meanwhile, rhenium–osmium isotopes show the asphalts are formed in 192+30/−45 Ma, which is similar to the J_1k sedimentation time. The asphalts contain coal macerals and probably derived from the asphaltene precipitated by the J_1k coal during the early coalification. The low abundance of 25-norbornanes with a non- or slight petroleum biodegradation degree indicates the asphalt was generated relatively late and migrated into the J_2y formation along the faults, possibly accompanied by the striking activities of the Altyn Tagh Fault during the Neotectonics movement. This study provides evidence for the J_1k coal-bearing strata serving as the effective source rock in the Ruoqiang Sag and increases confidence for Jurassic petroleum exploration in the Southeast Depression of the Tarim Basin. The structural and lithological traps near hydrocarbon source stoves, where Jurassic strata were

deeply buried and far from the Altyn Tagh Range, are favorable oil and gas exploration targets.

KEYWORDS

Ruoqiang Sag, Jurassic source rock, asphalt, hydrocarbon accumulation, Re-Os isotopic dating

1 Introduction

The Tarim Basin (Figure 1A) is the largest inland hydrocarbon-bearing basin in China, and it has great potential for petroleum exploration. The Southeast Depression of the Tarim Basin is located in the southeast of the Tarim Basin, covering an area of approximately 100,000 km^2, and has no industrial oil and gas accumulations. Up to now, only eight wells have been drilled, and two wells have obtained oil and gas, both in the Jurassic strata. A 30-m gas logging anomaly was found in the Jurassic of the RC1 well, and the QD1 well drilled Jurassic asphalt in 2016. Meanwhile, the Ruoqiang Sag has active hydrocarbon shows in the Jurassic outcrops, such as Qiemo Coalmine, Qigeleke, Ashahantuohai, and Jianggelesayi, which are oil seeds, oil traces, and asphalt veins (Chen and Hu, 1996). Previous studies on the Jurassic strata mainly focused on sedimentary characteristics, stratigraphic sequences, tectonic evolution, and petroleum geological conditions (Wang et al., 2000). The oil-source correlation was analyzed with Jurassic oil seeds and oil sands found in the Ruoqiang Sag (Xu et al., 1994; Chen and Hu, 1996). However, the few studies carried out on the regional source rock and hydrocarbon accumulation, which suggested that the source rock was from the Ordovician or directly from the J_2y lacustrine mudstone (Huang et al., 2013), were controversial. With the investment in regional petroleum exploration in recent years, the seismic work and drilling wells have revealed that the Jurassic is thick with a maximum sedimentary thickness of more than 1500 m, and Jurassic source rocks of J_1k and J_2y formations are good quality and well-developed in the outcrops and drilling wells. Many Jurassic asphalts were drilled in the QD1 well and are evidence of oil and gas generation, migration, and hydrocarbon accumulation, and can provide important research materials for regional petroleum geology.

The asphalt contains a large amount of heavy organic matter that can be analyzed for oil and source comparison and hydrocarbon accumulation by organic and inorganic geochemical methods, such as carbon isotopes, biomarkers, and main and trace elements (Moldowan et al., 1985; Curiale, 1986; Jacob, 1989; Hwang et al., 1998; Guckert and Mossman, 2003; Liao et al., 2015). The asphaltene of crude oils has over 90% of Re and Os elements due to their organophilic characteristics (Mahdaoui et al., 2013) and almost represents the entire crude oil isotopic composition of Re and Os (Selby et al., 2007). The organic-rich geological samples related to hydrocarbon accumulation, such as source rocks and asphalt, can be directly tested and analyzed by Re and Os isotope dating for petroleum accumulation geochronology (Selby and Creaser, 2005; Liu et al., 2018; Ge et al., 2020; Wu et al., 2021). In this study, the asphalts were researched to explore the possible hydrocarbon sources and accumulation processes in the Ruoqiang Sag, combined with the source rocks of the drilling core and outcrops.

2 Regional geology

The Southeast Depression of the Tarim Basin is distributed in a northeast-to-southwest direction (Figure 1A), adjacent to the Tadong Low Rise and Tangguzibas Sag bounded in the north by the Cherchen Fault (Figure 1B). It borders the Tiekelike Upfaulted Zone, the Altyn Tagh Range, and the Qaidam Basin by the left-lateral Altyn Fault in the south. The depression is divided into four secondary tectonic units, which are Minfeng Sag, Jiemo High, Ruoqiang Sag, and Luobuzhuang High from west to east. The Ruoqiang Sag is located in the central-eastern section of the depression and bounded by the Cherchen Fault in the north and the Altyn Tagh Range in the south. The sag is nearly diamond shaped, with an area of approximately 0.255 million square kilometers.

The three QD1, RC1, and RC2 wells are drilled in the Ruoqiang Sag (Figure 1B), and all encounter the Jurassic strata. From bottom to top, the regional strata exposed by outcrops and drilling wells are the Proterozoic, Jurassic, Cretaceous, Paleocene, Neoproterozoic, and Quaternary, with a large number of strata missing from Cambrian to Triassic. The Proterozoic has the main lithology of the variegated granite and dark gray gabbro. The Jurassic deposited above the Paleozoic basement with a set of coal-bearing sediments, including the fluvial and lacustrine facies, and is divided into Shalitash (J_1s) and Kangsu (J_1k) formations of the Lower Jurassic, Yangye (J_2y) and Targa (J_2t) formations of the Middle Jurassic (Figure 2), and a Kuzigongsu (J_3k) Formation of the Upper Jurassic from bottom to top.

During the strong faulting period of the Early Jurassic (Wang et al., 2005), the J_1s strata rapidly deposited along the marginal faults NE toward the Ruoqiang Sag as an alluvial fan or braided-river delta and have the lithology of gray conglomerate and sandstone sandwiched with gray siltstone. In the late Early Jurassic, the J_1k strata deposited a set of coal-bearing sediments with the sedimentary facies of braided-river delta and shallow coastal lakes (Ritts and Biffi, 2000; Yue et al., 2004). The J_1k lithology is characterized by conglomerate, coarse to fine sandstone, gray-black carbonaceous mudstone, and coal. During the Middle Jurassic, the paleo-lacustrine basin continued to expand, and the J_2y strata were deposited under a hemi-deep or deep lake environment (Cheng et al., 2008). The J_2y lithology is sandstone and mudstone interbedded with varying thicknesses, interbedded with dark mudstone and carbonaceous mudstone. However, the climate became hot and arid in the late Middle Jurassic, and the J_2t developed fluvial or fan-deltaic facies sediments (Li, 1998), mainly composed of purple-red sandstone and conglomerate with a thickness of 277–302.7 m. As the Upper Jurassic, the J_3k strata have been eroded, and the residual thickness is relatively thin with the lithology of purple-red or brownish-red sandstone and mudstone. In the Late Jurassic, the Lhasa terrane collided with

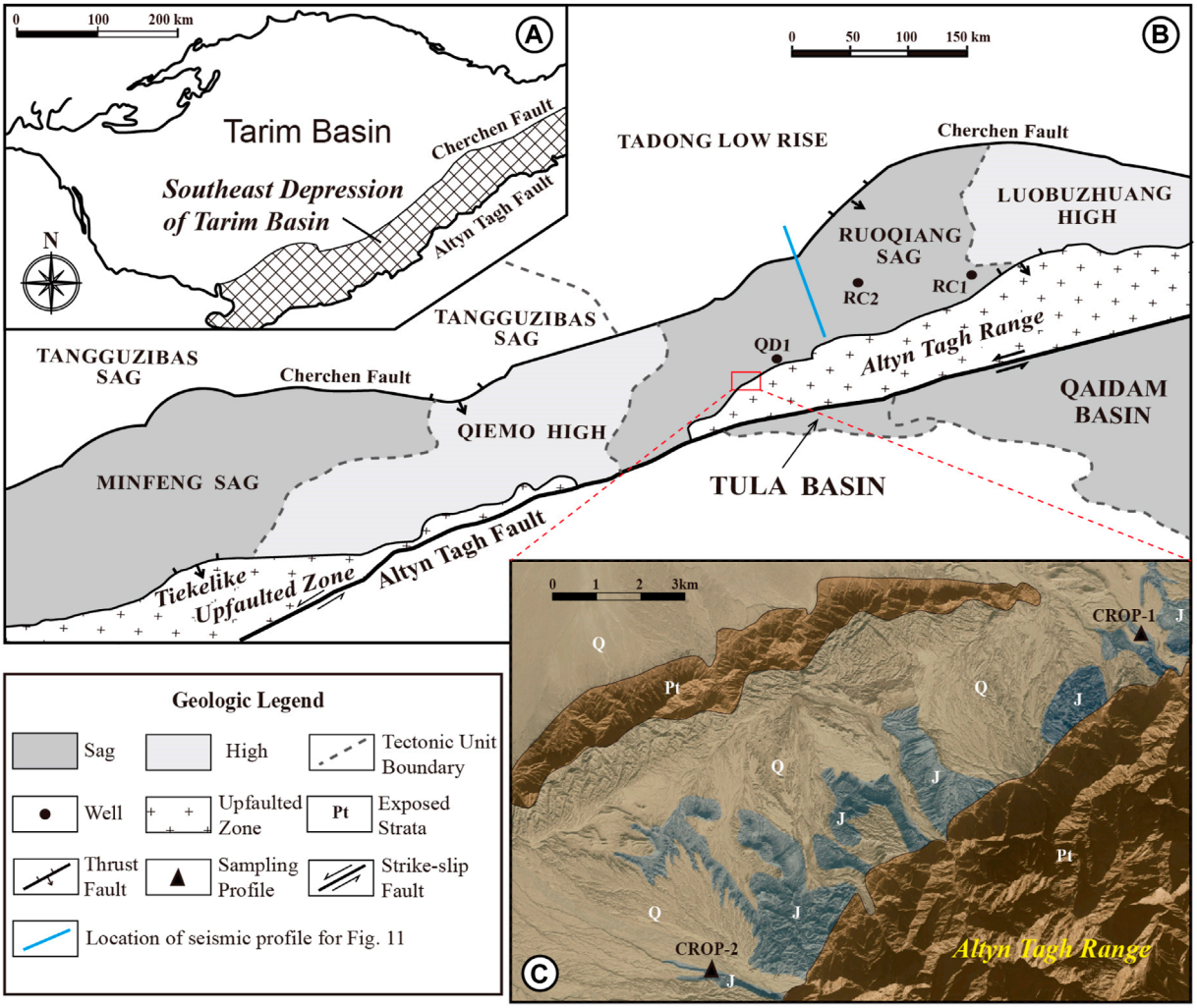

FIGURE 1
Map of the study area showing the location of Ruoqiang Sag, outcrops, and strata. **(A)** Location of the Southeast Depression of the Tarim Basin; **(B)** tectonic units of the Southeast Depression of the Tarim Basin and wells in the Ruoqiang Sag; **(C)** location of three outcrops in this study.

the Qiangtang terrane (Li et al., 2002; Liu et al., 2003), resulting in the overall Southeast Depression of the Tarim Basin uplifting with extensive absence of syn-depositional sediments. The Lower Cretaceous has a restricted distribution and is composed of red medium-coarse-grained clasolite. The Cenozoic strata are a set of sandstone and mudstone deposits of braided fluvial facies (Cheng et al., 2008) and in angular unconformable contact with the underlying strata, with a thickness of less than 3,914 m. The Quaternary is mainly composed of thin aeolian sediments. From the perspective of lithology and burial depth, the regional hydrocarbon sources can only come from the J_1k and J_2y formations.

3 Samples and methods

Twenty-five source rock samples and five asphalt samples shown in Figure 2 were collected and marked. The source rock samples include 16 drilling cores (marked from QD-1 to QD-16) and nine outcrop samples, six from Outcrop-1 (marked from C1-1 to C1-6) and three from Outcrop-2 (marked from C2-1 to C2-3), among which the C1-6 is only J_1k coal sample collected from Outcrop-1 (Figure 1C). The others were mudstone, including the 15 J_2y and 9 J_1k samples. In order to ensure the purity of the asphalt, the asphalt samples were selected from the fractures of the Yangye Formation in the QD1 well and marked from SA-1 to SA-5.

Four experiments were completed in the State Key Laboratory of Oil and Gas Resources and Prospecting of China University of Petroleum (Beijing). Two asphalt samples were polished and analyzed for macerals and vitrinite reflectance using DM4P-Leica DM 4 P& MSP9000C polarization microscopes. Organic carbon content and rock pyrolysis experiments on 25 samples were done with a Leco CS230 analyzer and an OGE-II oil and gas pyrolyzer, respectively. A 20-g powdered sample was slowly mixed with excess HCl; heated to 80°C to remove the inorganic carbon;

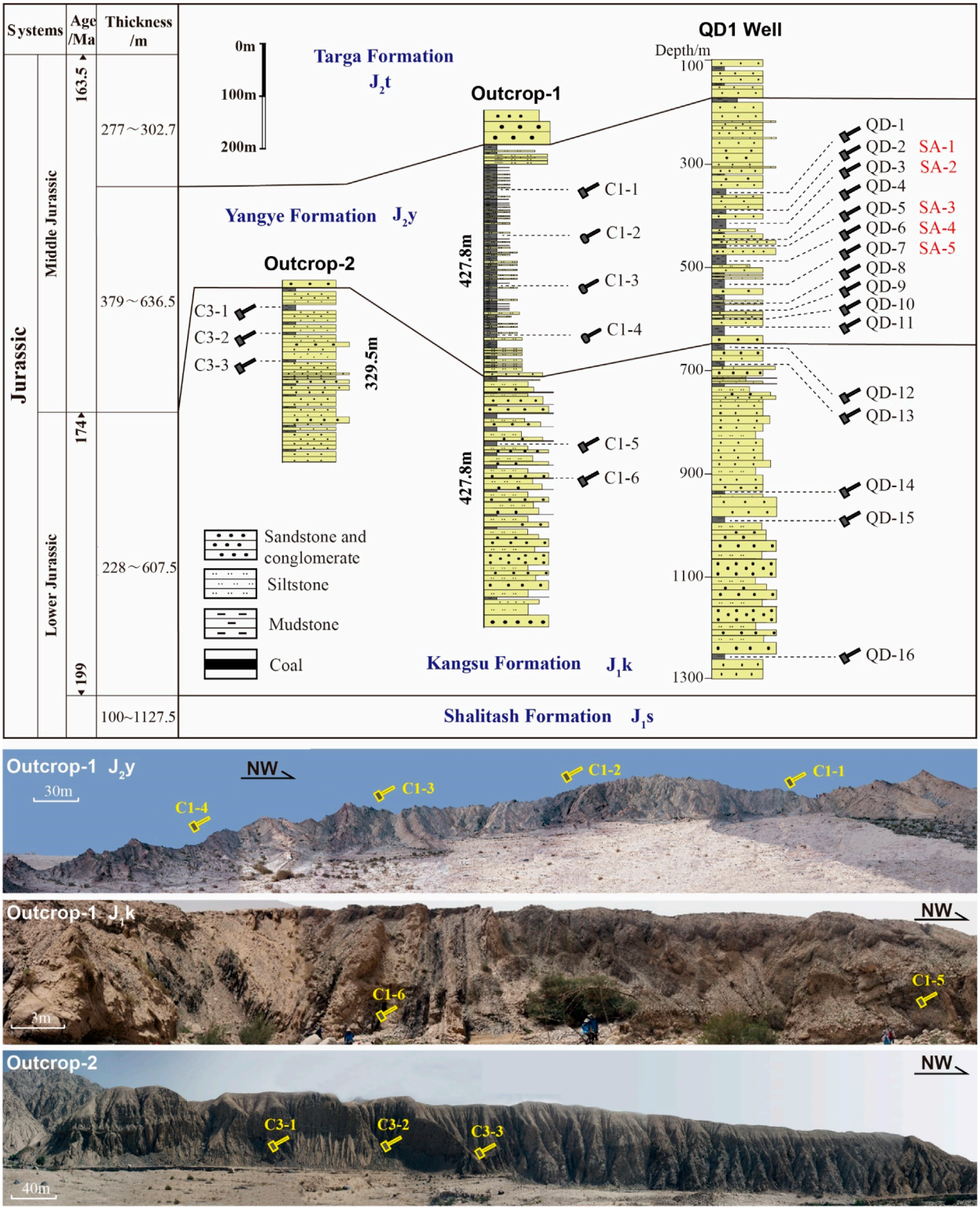

FIGURE 2
Jurassic lithology histogram and samples in the QD1 well and two outcrops. Source rock samples are marked with black and yellow in the outcrop photos, while asphalt samples are marked in red with the same depths as the source rock samples in front of them.

and then washed, dried, and placed in the carbon and sulfur analyzer for organic carbon determination. The rock pyrolysis experiments were completed in the OGE-II oil and gas evaluator. The hydrocarbons emitted from the powdered samples during the pyrolysis process were detected in the carrier gas stream using a hydrogen flame ionization detector. Six samples were

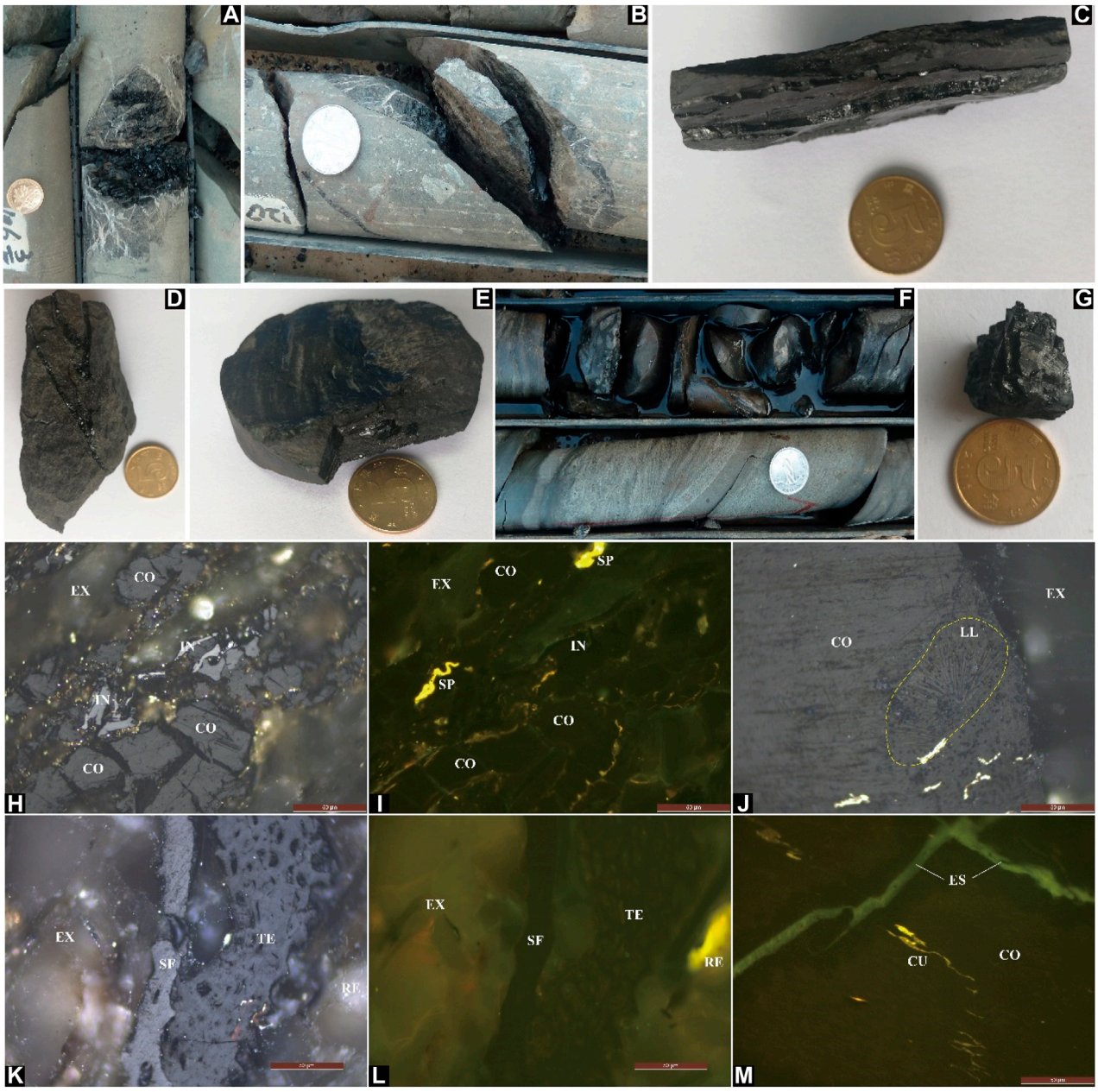

FIGURE 3
Jurassic asphalt photographs in the cores and under the microscope. The core photographs of **(A–G)** are from QD1 depth sections of 229.4 m, 363.7 m, 431.0 m, 425.7 m, 496.3 m, 459.5 m, and 366.0 m, respectively. Photographs of **(H, J, K)** are taken under oil-immersed reflected light, while ultraviolet light is used to take the photographs of **(I, L, M)**. The **(J–M)** are from Sample SA-3, while **(H, I)** are from Sample SA-4. The shown maceral components include exinite (EX), collinite (CO), sporophyte (SP), leaf lobes (LL), semifusinite (SF), telinite (TE), cutinite (CU), exsudatinite (ES), and resinite (RE).

subjected to a gas chromatography-mass spectroscopy (GC-MS) experiment, including one J_1k coal and one J_1k mudstone, two J_2y mudstones, and two J_2y asphalt samples. The saturate fraction was performed on a Thermo Fisher Trace-DSQII instrument with an HP-5MS fused silica column (60 m × 0.25 mm × 0.25 μm). The initial temperature was held at 50°C for 1 min, programmed to increase to 100°C at 15°C/min, then to 200°C at 2°C/min, 315°C at 1°C/min, and held for 20 min. The flow rate of carrier gas was 1 mL/min.

Rare earth element analyses of eight samples, including two asphalts of 1 J_2y and 1 J_1k, one J_1k coal, three J_2y mudstone, and two J_1k mudstone samples, were done in the Beijing Institute of Nuclear Industry Geology. A 0.05 g powdered sample was placed in a closed sampler, and 1 mL HF and 0.5 mL HNO_3 were added, allowed to dissolve, and heated to 185°C. The mixed solution was placed on an electric heating plate for evaporation and then sealed with nitric acid for dissolution after removing hydrofluoric acid. Finally, the diluted solution was analyzed on a Thermo Scientific

TABLE 1 TOC, rock-eval pyrolysis, and vitrinite reflectance data on Jurassic samples in the Ruoqiang Sag.

Sample	Lithology	Location	Depth (m)	Formation	TOC (%)	S_1 (mg/g)	S_2 (mg/g)	S_3 (mg/g)	T_{max} °C	OI	HI	S_1+S_2 (mg/g)	Ro (%)
QD-1	Mudstone	QD1 well	312.8	J_2y	4.02	0.86	10.77	2.04	422	50.77	268.04	11.63	0.34
QD-2	Mudstone	QD1 well	366.0	J_2y	2.88	1.81	21.10	4.56	424	158.61	734.02	22.91	0.33
QD-3	Mudstone	QD1 well	385.0	J_2y	4.02	1.81	21.10	4.47	424	111.25	525.21	22.91	0.37
QD-4	Mudstone	QD1 well	417.0	J_2y	5.35	0.17	25.30	1.32	416	24.69	473.25	25.47	0.36
QD-5	Mudstone	QD1 well	425.0	J_2y	9.20	2.93	15.99	1.06	408	11.52	173.85	18.92	0.38
QD-6	Mudstone	QD1 well	459.5	J_2y	3.50	0.10	14.57	0.99	425	28.33	416.88	14.67	0.37
QD-7	Mudstone	QD1 well	502.8	J_2y	4.19	0.16	27.78	1.03	412	24.58	662.85	27.94	0.37
QD-8	Mudstone	QD1 well	534.9	J_2y	7.20	0.15	28.40	1.25	425	17.36	394.44	28.55	0.33
QD-9	Mudstone	QD1 well	556.0	J_2y	4.06	0.17	25.65	1.30	410	31.99	631.15	25.82	0.38
QD-10	Mudstone	QD1 well	564.9	J_2y	1.71	0.05	3.40	1.08	420	63.16	198.83	3.45	0.34
QD-11	Mudstone	QD1 well	582.0	J_2y	4.60	0.25	33.83	1.40	413	30.43	735.43	34.08	0.41
QD-12	Mudstone	QD1 well	608.4	J_1k	1.17	0.40	6.80	0.86	430	73.50	581.20	7.20	0.39
QD-13	Mudstone	QD1 well	643.3	J_1k	4.94	0.16	21.90	1.38	425	27.92	443.14	22.06	0.42
QD-14	Mudstone	QD1 well	880.0	J_1k	1.97	0.90	6.20	0.80	433	40.69	315.36	7.10	0.45
QD-15	Mudstone	QD1 well	923.1	J_1k	11.15	0.79	43.47	2.48	413	22.24	389.87	44.26	0.42
QD-16	Mudstone	QD1 well	1,211.0	J_1k	2.97	0.03	4.15	3.58	436	120.46	139.64	4.18	0.57
C2-1	Mudstone	Outcrop-2	-	J_1k	4.67	0.03	3.32	3.28	430	70.24	71.13	3.35	0.42
C2-2	Mudstone	Outcrop-2	-	J_1k	1.12	0.10	3.38	3.16	438	282.14	301.61	3.48	0.43
C2-3	Mudstone	Outcrop-2	-	J_1k	1.11	0.05	3.20	2.78	420	251.58	289.14	3.24	0.45
C1-1	Mudstone	Outcrop-1	-	J_2y	4.42	0.06	4.71	4.00	436	90.44	106.50	4.77	0.37
C1-2	Mudstone	Outcrop-1	-	J_2y	4.58	0.07	6.22	4.86	435	106.06	135.75	6.29	0.36
C1-3	Mudstone	Outcrop-1	-	J_2y	3.97	0.04	3.83	3.73	435	93.89	96.41	3.87	0.37

(Continued on the following page)

10.3389/feart.2024.1371358

TABLE 1 (*Continued*) TOC, rock-eval pyrolysis, and vitrinite reflectance data on Jurassic samples in the Ruoqiang Sag.

Sample	Lithology	Location	Depth (m)	Formation	TOC (%)	S_1 (mg/g)	S_2 (mg/g)	S_3 (mg/g)	T_{max} °C	OI	HI	S_1+S_2 (mg/g)	Ro (%)
C1-4	Mudstone	Outcrop-1	-	J_2y	3.83	0.05	4.79	3.22	434	84.04	125.02	4.84	0.41
C1-5	Mudstone	Outcrop-1	-	J_1k	1.25	7.78	2.25	1.48	430	118.68	180.19	10.02	0.38
C1-6	Coal	Outcrop-1	-	J_1k	23.00	1.35	71.25	4.73	423	20.57	309.78	72.60	0.49
SA-3	Asphalt	QD1 well	425.0	J_2y	-	-	-	-	-	-	-	-	0.41
SA-4	Asphalt	QD1 well	459.5	J_2y	-	-	-	-	-	-	-	-	0.54

S_1-free hydrocarbons; S_2-hydrocarbons from pyrolysis of kerogen; S_3-release of trapped CO_2; Ro is the average vitrinite reflectance from 40 measurement points; OI, $S_3\times100$/TOC; HI, $S_2\times100$/TOC.

high-resolution inductively coupled plasma mass spectrometer of ELEMENT XR, and the rare earth element content was calculated with the external standard method.

The rhenium–osmium isotopes of asphalt were tested using the same five samples (SA-1 to SA-5) in two laboratories. Five samples (marked from SA-1_d to SA-5_d) were tested at Durham University, United Kingdom, and six samples (marked from SA-1_c to SA-5_c; SA-3_c was further divided into two parts and labeled as SA-3_{c1} and SA-3_{c2}) were tested in the National Geological Experimental Test Center of the Chinese Academy of Geological Sciences. The asphalt samples were ground into a 4~5 mm powder, 0.1–0.2 g was weighed into a Carlos tube, and reverse aqua regia (HNO_3+3 HCl) and 2 mL of 30% H_2O_2 solution were added as the dissolution reagent. After adding a certain amount of diluent, the tube was sealed. Then, the samples were dissolved with a stage heating method (first, heated to 120°C, stabilized for about 1 h; then heated to 160°C, stabilized for about 2 h; and finally raised to 200°C and stabilized for 24 h). Then, the tube was opened after freezing, and Os was separated and purified by *in situ* direct distillation and microdistillation. After that, 5 mol/L NaOH solution was added, and acetone was used to extract Re. The acetone was evaporated to dryness at low temperature, and then, HNO_3 and H_2O_2 were added to destroy the organic phase to separate the Re. The separated and purified Re and Os were measured by a Thermo Fisher Triton Plus Negative Ion Thermal Ionization Mass Spectrometer (N-TIMS).

4 Results

4.1 Maceral composition of asphalt

In the QD1 drilling core, the asphalts are filled in the fractures (Figures 3A,B) or as thin layers in the Jurassic mudstone (Figures 3C–E), and an oil slick occurs when soaked in water (Figure 3F). The fresh asphalt is bright black with visible conchoidal fractures (Figure 3G). Under the microscope, the asphalt contains three obvious groups of macerals—vitrinite, exinite, and inertinite. Overall, the macerals are mainly composed of vitrinite, especially the collinite (Figure 3H) and telinite (Figure 3K), which appear dark gray under oil-immersed reflected light and brownish-black under fluorescence. The exinite components are rich and show grayish black under oil-immersed reflected light (Figures 3H,J,K) and orange to bright yellow under fluorescence. The exinites are dominated by sporophyte (Figure 3I), cutinite (Figure 3M), and resinite (Figure 3L). The inertinite components are less abundant with fusinite and semifusinite (Figure 3K) and show grayish-white under oil-immersed reflected light (Figure 3H) and black under fluorescence (Figure 3I). Some exsudatinites are visible in cracks and residual pore cavities of the microcomponent (Figure 3M), and even fossilized plant leaf lobes (Figure 3J) and flow morphology of macerals are visible (Figures 3J,L). Therefore, the Jurassic asphalt retains the coal macerals and is related to the Jurassic coal.

4.2 Rock-eval pyrolysis

In the 25 samples (Table 1), the total organic carbon (TOC) of J_1k and J_2y are both greater than 1.0% (1.17–23.00%), making them

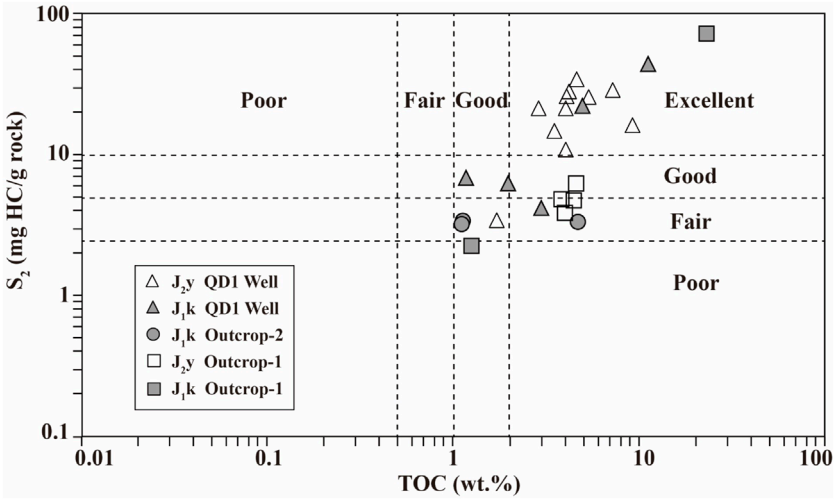

FIGURE 4
TOC vs. S_2 crossplot (Dembicki, 2009) for quality of the Jurassic source rock in the QD1 well and outcrops (for location, see Figure 1B).

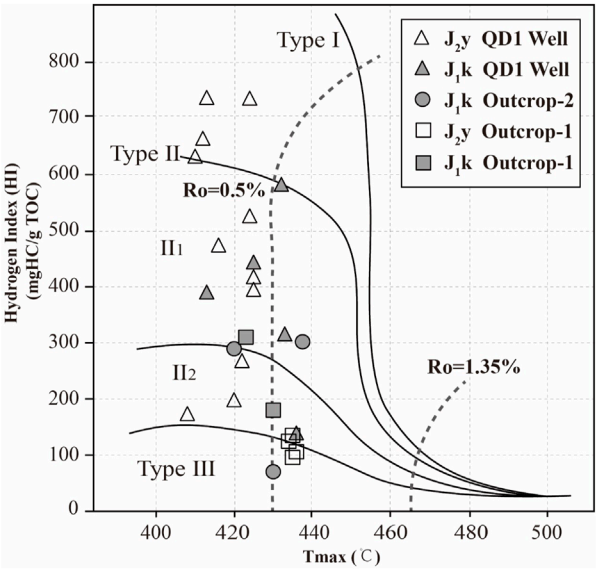

FIGURE 5
T_{max} vs. hydrogen index crossplot for quality evaluation of the Jurassic source rock in the Ruoqiang Sag.

good to excellent source rocks (Figure 4). The J_1k samples are poor to excellent source rocks with a pyrolysis parameter (S_2) ranging from 2.25 to 71.25 mg HC/g rock. The J_2y samples have higher quality than the J_1k source rock with an S_2 ranging from 3.40 to 33.83 mg HC/g Rock. From the T_{max} vs. HI crossplot (Figure 5), J_2y source rocks have three kerogen types while J_1k has kerogen of the II and III types. Based on the comprehensive pyrolysis parameters, the J_2y source rocks have better quality than J_1k. The testing samples have an Ro from 0.33% to 0.57%, which indicates an immature to low maturity stage. Two Ro values of asphalt are 0.41% and 0.54%, close to the J_1k Ro values (Ro = 0.38%–0.57%, average = 0.44%) and above the J_2y Ro values, which range from 0.33% to 0.41% with an average of 0.37%.

4.3 Rare earth element characteristics

The total rare earth element (REE) concentrations of J_2y mudstone are the highest, from 275.59 to 317.45 μg/g (Table 2), followed by those of the J_1k mudstone at 139.20–143.77 μg/g. J_1k coal has an REE concentration of 68.71 μg/g, which is slightly higher than the asphalt (35.88–41.92 μg/g). Light rare earth elements (LREEs) are more enriched in all samples than heavy rare earth elements (HREE), and the LREE/HREE ratios of J_2y mudstone are from 9.27 to 9.70, which is higher than the 6.37–6.95 of J_1k mudstone, higher than the 4.73 of J_1k coal, and higher than the 1.45–2.04 of the asphalt. The chondrite normalization values are after Boynton (1984), and all of the chondrite-normalized REE curves show the right-sloping characteristics with LREE enrichment. However, the curves gradually flatten from the J_2y mudstone to J_1k mudstone to J_1k coal and then to asphalt (Figure 6). All the samples show pronounced negative Eu anomalies. The δEu values of asphalt value vary from 0.84 to 0.92, close to those of J_1k mudstone and coal, ranging from 0.83 to 0.89, much higher than J_2y values of 0.70–0.80. The Ce anomalies are weak and relatively close, with slightly lower δCe values of asphalt, ranging from 0.90 to 0.98.

The J_2y/Ho ratios vary from 23.80 to 27.50, which is lower than those of J_1k mudstones (30.67–31.50) and asphalt Y/Ho ratios of 30.04–44.69, which are close to the 36.3 of J_1k coal (Table 2). The $(Ce/Yb)_N$, $(La/Yb)_N$, $(La/Sm)_N$, and $(Gd/Yb)_N$ ratios of J_2y mudstone are 8.84–9.11, 11.39–11.95, 3.32–3.47, and 2.22–2.39, much higher than those of J_1k samples, which are 3.18–5.96, 4.49–7.63, 2.90–3.57, and 1.00–1.78, respectively. The corresponding ratios of asphalt samples were 0.75–0.95, 1.15–1.17, 1.08–1.15, and 0.77–1.07, respectively.

TABLE 2 Rare earth elements of the Jurassic samples in the Ruoqiang Sag.

Sample	ΣREE	LREE	HREE	LREE/HREE	$(Ce/Yb)_N$	$(La/Yb)_N$	δEu	$(La/Sm)_N$	$(Gd/Yb)_N$	δCe	Y/Ho
SA-3	35.88	24.09	11.79	2.04	0.95	1.17	0.92	1.15	0.77	0.91	30.04
SA-4	41.92	24.78	17.14	1.45	0.75	1.15	0.84	1.08	1.07	0.90	44.69
QD-3	275.59	249.83	25.76	9.70	9.11	11.95	0.70	3.47	2.31	0.97	27.50
QD-6	317.45	286.53	30.92	9.27	8.85	11.61	0.80	3.32	2.39	0.96	24.93
QD-8	297.29	269.21	28.08	9.59	8.84	11.39	0.77	3.42	2.22	0.98	23.80
C1-6	68.71	56.73	11.98	4.73	3.18	4.49	0.83	3.57	1.00	0.96	36.25
QD-13	139.20	120.32	18.88	6.37	5.14	6.72	0.89	3.02	1.62	0.98	31.50
QD-14	143.77	125.69	18.08	6.95	5.96	7.63	0.84	2.90	1.78	0.98	30.67

$\delta Eu = Eu_N/(Sm_N \times Gd_N)^{1/2}$; $\delta Ce = Ce_N/(La_N \times Pr_N)^{1/2}$.

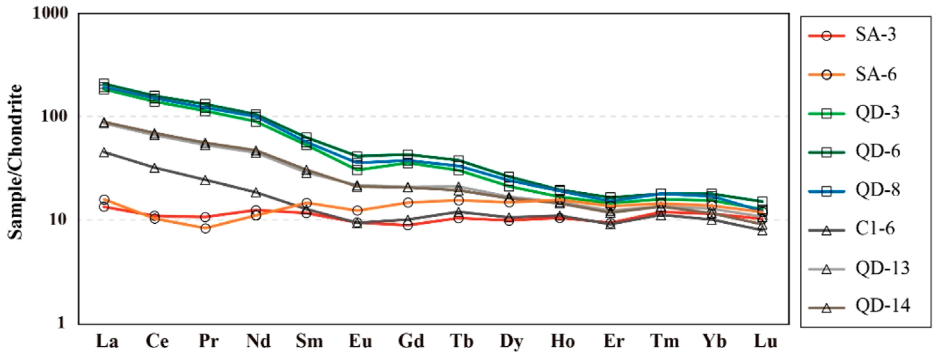

FIGURE 6
Chondrite-normalized REE patterns of the Jurassic samples in the Ruoqiang Sag.

4.4 Organic geochemistry characterization

The Jurassic alkanes are primarily distributed from *n*-C_{12} to *n*-C_{35}, with *n*-C_{25} as the single dominant *n*-alkane on the *m/z* 85 fragmentation diagram (Figure 7). The *n*-alkane composition has a distinct odd-even dominance with the odd *n*-alkane abundance higher than the even ones. The J_1k samples have an OEP (2.22–2.47) and CPI (1.38–1.75) similar to those of asphalt samples (OEP: 2.78–4.09; CPI: 1.84–2.30) and significantly lower than those of J_2y samples, which have OEP values of 5.02 and 5.19 and CPI values of 3.04 and 3.10, respectively (Table 3). The Pr/Ph ratios of Jurassic samples are all higher than 2.5, and the Pr/Ph values of the two J_2y mudstones are 3.01 and 3.62, slightly higher than that of the J_1k mudstone (2.85). However, the Jurassic mudstone Pr/Ph values are significantly lower than those of J_1k coal (5.12) and asphalt (5.09–5.85).

Quantified using *m/z* 191, the relative abundances of tricyclic and tetracyclic terpenoids are generally low, while the pentacyclic triterpenes are abundant, especially the C_{29} to C_{32} hopanes (Figure 7). The Ga/C_{30}H ratios range from 0.03 to 0.09 for all Jurassic samples (Table 3). The Ts/(Ts+Tm) values of the J_1k coal and mudstone are 0.78 and 0.90, respectively, significantly higher than those of the two J_2y mudstones (0.44 and 0.56). The asphalt extracts also have high Ts/(Ts+Tm) ratios, 0.52 and 0.56 for the two samples, respectively.

From the *m/z* 217 sterane compounds (Figure 7; Table 3), C_{27}, C_{28}, and C_{29} conventional steranes are distributed in a "V" shape with the abundance of C_{29}ααR sterane higher than C_{27}ααR and C_{28}ααR steranes. The asphalt extracts have a slightly higher proportion of C_{29} steranes and a lower proportion of C_{28} steranes, distinguished from the similar sterane compositions of the J_1k and J_2y. Meanwhile, the Jurassic extract values from the two maturity indexes of C_{27} (DSt/St) and C_{29} 20s/(20s+20r) are close. The J_1k C_{29} ββ/(αα+ββ) values are 0.51 and 0.46, higher than two J_2y extracts (0.27 and 0.38) and close to two asphalt values of 0.52 and 0.50.

4.5 Rhenium–osmium isotopes

The Jurassic asphalts have low Re and Os contents (Table 4). The Re content is between 0.82 and 11.36 ppb, with Os content varying from 26.82 to 131.85 ppt (Table 4), which is different from the Re and Os composition of the continental crust (Re content less than 1 ppb, and Os content less than 50 ppt). The $^{187}Re/^{188}Os$

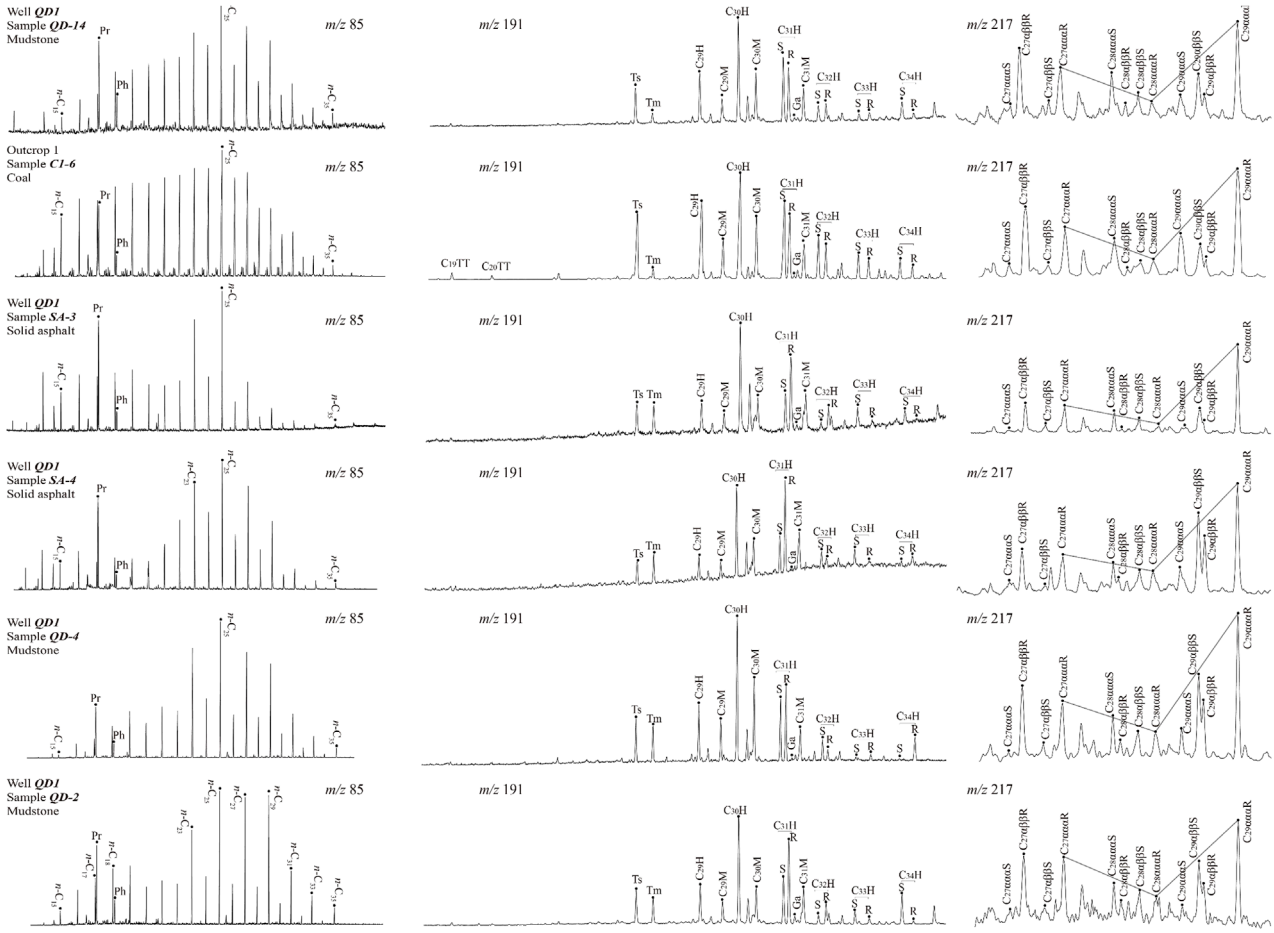

FIGURE 7
GC-MS characteristics of the Jurassic extracts in the Ruoqiang Sag.

values of asphalt vary from 58.7 to 576.1, while the $^{187}Os/^{188}Os$ ratio is in the range of 1.56–3.09 (Table 4). The linear fitting between $^{187}Re/^{188}Os$ and $^{187}Os/^{188}Os$ is relatively high with an R^2 of 91.8%, and the asphalt forming age is calculated to be 192 +30/−45 Ma with the isochrone slopes (Figure 8).

5 Discussion

5.1 Oil–source correlation

The rare earth elements have very similar and highly stable chemical properties that are not easily affected by metamorphism and can be used to determine the depositional environment, type, and origin of source rock (Condie, 1991; Tribovillard et al., 2006). The J_2y mudstones have significantly higher REE content and $(La/Sm)_N$ and $(Gd/Yb)_N$ ratios than the J_1k, indicating that the J_2y deposited with higher LREE and HREE fractionation under a warmer and wetter environment (Fleet, 1984). The J_1k coal and asphalt have similar REE content, reflecting a similar sedimentary environment. The J_2y REE curves appear to have steeper right-sloping characteristics than the J_1k ones (Figure 6) and have higher ratios of $(La/Yb)_N$ and $(Ce/Yb)_N$, with the LREE higher than HREE. Compared to braided-river delta and shallow coastal lakes of J_1k sedimentary environment close to the sediment source (Cheng et al., 2008), the J_2y distal sediments have fine particles and strong adsorption with the REE characteristics mentioned above. The δCe values of all samples are relatively close, with similar oxidizing properties of depositional environments (Elderfield and Pagett, 1986). However, the δEu values of asphalt and J_1k samples are significantly higher than the J_2y ones, reflecting the differences in sedimentary waters (Hass et al., 1995). The rare earth elements Y and Ho have very similar geochemical properties, but Y has an unusually low affinity for Fe oxides compared to Ho (Gong et al., 2021). It is clear that the J_2y Y/Ho values are higher than those of the asphalt and J_1k samples, indicating the J_2y depositional environment was more reduced. Therefore, combined with the REE partition curves and ratio relationships (Figure 6; Table 2), the asphalts have a closer relationship with the J_1k, especially the J_1k coal, suggesting that they are more closely related.

The Jurassic biomarker compounds show the characteristics of high Pr/Ph, high C_{29} steroid, and low abundance of tricyclic terpene alkanes, highly consistent with the Jurassic source rocks studied by previous researchers (Hendrix et al., 1995). The asphalt extracts have

10.3389/feart.2024.1371358

TABLE 3 Summary biomarker parameters for Jurassic sample extracts in the Ruoqiang Sag.

Sample	QD-2	QD-4	QD-14	C1-6	SA-3	SA-4
	J_2y mudstone	J_2y mudstone	J_1k mudstone	J_1k coal	J_2y asphalt	J_2y asphalt
Dominant *n*-alkane	25	25	25	25	25	25
CPI	3.10	3.04	1.75	1.38	2.30	1.84
OEP	5.19	5.02	2.47	2.22	4.09	2.78
Pr/Ph	3.62	3.01	2.85	5.12	5.09	5.85
Ts/(Ts+Tm)	0.56	0.44	0.78	0.9	0.52	0.53
G/C_{30}H	0.09	0.19	0.04	0.07	0.07	0.06
C_{31} 22S/(22S+22R)	0.36	0.33	0.54	0.58	0.34	0.45
C_{32} 22S/(22S+22R)	0.32	0.54	0.49	0.55	0.32	0.33
C_{27} (DSt/St)	0.10	0.36	0.22	0.17	0.20	0.25
C_{29} 20s/(20s+20r)	0.32	0.28	0.25	0.28	0.29	0.29
C_{29} ββ/(αα+ββ)	0.27	0.38	0.51	0.46	0.52	0.50
C_{27} *	0.32	0.28	0.31	0.28	0.25	0.24
C_{28} *	0.21	0.23	0.24	0.23	0.17	0.16
C_{29} *	0.47	0.50	0.45	0.48	0.57	0.60
C_{27}/C_{29}	0.68	0.56	0.70	0.59	0.44	0.40
C_{28}/C_{29}	0.45	0.45	0.54	0.49	0.30	0.27

CPI, $0.5 * (n\text{-}C_{25}+n\text{-}C_{27}+n\text{-}C_{29}+n\text{-}C_{31}+n\text{-}C_{33}) * [1/(n\text{-}C_{24}+n\text{-}C_{26}+n\text{-}C_{28}+n\text{-}C_{30}+n\text{-}C_{32})+ 1/(n\text{-}C_{26}+n\text{-}C_{28}+n\text{-}C_{30}+n\text{-}C_{32}+n\text{-}C_{34})]$; TAR = $(n\text{-}C_{27}+n\text{-}C_{29}+n\text{-}C_{31})/(n\text{-}C_{15}+n\text{-}C_{17}+n\text{-}C_{19})$; OEP = $(n\text{-}C_{(Nmax-2)}+6 * n\text{-}C_{Nmax}+ n\text{-}C_{(Nmax+2)})/(4 * n\text{-}C_{(Nmax-1)}+ n\text{-}C_{(Nmax+1)})$; Pr/Ph, pristine/phytane; Ts/(Ts+Tm) = 18a(H)-22,29,30-trisnorneohopane/(18a(H)-22,29,30-trisnorneohopane +17a(H)-22,29,30-trisnorhopane); G/C_{30}H, gammacerane to C_{30} hopane; C_{31} 22S/(22S+22R) = 22S to (22S + 22R) ratios for C_{31} 17α-hopanes; C_{32} 22S/(22S+22R) = 22S to (22S + 22R) ratios for C_{32} 17α-hopanes; C_{27} (DSt/St) = 13β, 17α(H) - diasteranes 20S+20R] to 20S+20R isomers of C_{27} isosterane and C27 regular steranes; C_{29} ββ/(αα+ββ) = ββ to (αα+ββ) isomerization of C_{29} 20S and 20R regular steranes; C_{29} 20s/(20s+20r) = C_{29} 5a(H), 14a(H), and 17a(H) sterane 20S/(20S + 20R); C_{27} * , C_{28} * , and C_{29} * , relative percentages of C_{27}, C_{28}, and C_{29} regular steranes, respectively; C_{27}/C_{29}, regular sterane ratio of C_{27} to C_{29}; C_{28}/C_{29}, regular sterane ratio of C_{28} to C_{29}.

similar Pr/Ph ratios with J_1k coal, which suggests they have similar depositional environment oxidizing properties and closer affinities. The peak alkane is *n*-C_{25} for all samples (Figure 7; Table 3), reflecting that the regional Jurassic organic matter sources are highly related to terrestrial sources. In terms of the *m/z* 217 sterane compounds (Table 3), the J_2y extracts have similar C_{27} regular sterane content with the J_1k and slightly higher C_{27}/C_{29} regular sterane ratio and slightly lower C_{28}/C_{29} regular sterane ratio, indicating that the origins of J_2y organic matter have more algae (Volkman, 1986). The CPI and OEP of the Jurassic source rocks and asphalt are all greater than 1.0, suggesting that their thermal maturity is low. In contrast, the J_1k CPI and OEP values are lower than those of the J_2y (Table 3) and close to those of asphalt, indicating that the asphalts have similar thermal maturity to the J_1k. By the maturity-related biomarker parameters of Ts/(Ts+Tm), C_{31}22S/(22S+22R), and C_{32}22S/(22S+22R), the J_1k and asphalt have proximate maturity with biomarker parameters higher than those of the J_2y. By the C_{29} ββ/(αα+ββ) ratio, the J_1k has similar thermal maturity with asphalt but slightly higher than the J_2y extracts. Therefore, the Jurassic asphalts are more closely related to the J_1k.

Even if the source rock underwent hydrocarbon generation and expulsion processes, the Re-Os system can still remain closed and record its sedimentary age (Creaser et al., 2002). However, the isochronous age of asphalt Re-Os isotopes may reflect the sedimentary age of source rock or hydrocarbon migration/accumulation age, which mainly depends on the closure of the Re-Os isotopic system. If the Re-Os isotopic system is not closed with different Re and Os isotopes evenly mixed, then the asphalt Re-Os isochronous age represents the migration/accumulation age (Selby and Creaser, 2005). Using the plots of $^{187}Os/^{188}Os$ *versus* $^{187}Re/^{188}Os$, the age of the Jurassic asphalt is 192+30/−45 Ma, similar to the J_1k deposition time, suggesting that the asphalt is closely related to J_1k strata. It is obvious that the J_2y asphalt retains the Re-Os characteristics of J_1k coal, and the Re-Os isotope system is closed during the entire hydrocarbon generation and migration process.

TABLE 4 Rhenium–osmium data synopsis for Jurassic samples in the Ruoqiang Sag.

Sample	Re (ppb)	2σ	Os (ppt)	2σ	^{187}Os	2σ	$^{187}Re/^{188}Os$	2σ	$^{187}Os/^{188}Os$	2σ
$SA\text{-}1_d$	0.82	0.01	80.0	0.7	27.8	0.3	58.7	1.0	1.563	0.023
$SA\text{-}2_d$	2.85	0.01	79.5	0.7	25.5	0.3	222.3	2.8	2.317	0.034
$SA\text{-}3_d$	2.48	0.01	35.7	0.5	10.8	0.2	457.8	9.7	2.927	0.066
$SA\text{-}4_d$	11.36	0.03	131.8	1.2	39.2	0.4	576.1	6.0	3.093	0.042
$SA\text{-}5_d$	2.06	0.01	65.9	0.6	22.6	20.3	181.4	2.5	1.702	0.026
$SA\text{-}1_c$	1.56	0.01	32.9	0.1	8.5	0.1	229.1	2.9	1.984	0.013
$SA\text{-}2_c$	2.19	0.02	48.0	0.1	14.5	0.1	220.5	2.3	2.308	0.005
$SA\text{-}3_{c1}$	3.28	0.02	35.4	0.1	13.3	0.1	448.3	4.6	2.886	0.006
$SA\text{-}3_{c2}$	3.99	0.03	43.5	0.1	16.4	0.1	442.1	4.5	2.895	0.006
$SA\text{-}4_c$	3.66	0.03	43.6	0.1	15.6	0.1	405.9	4.2	2.761	0.007
$SA\text{-}5_c$	1.88	0.01	26.8	0.1	8.9	0.1	338.1	3.5	2.534	0.007

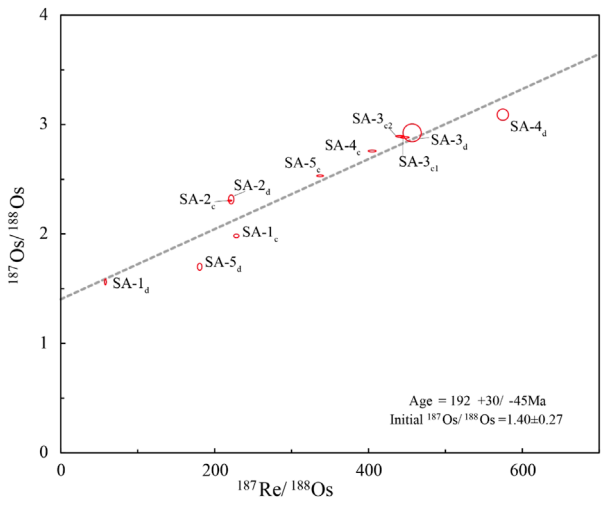

FIGURE 8
$^{187}Re/^{188}Os$ *versus* $^{187}Os/^{188}Os$ plots for the Jurassic solid asphalts.

More importantly, from the macerals, the Jurassic asphalt is mainly precipitated from exinite-rich components such as sporophytes, alginate, and resinite during the coalification. The asphalt precursor was mixed with vitrinite, inertinite, and other coal macerals and sometimes, flow traces are visible under the microscope (Figures 3I,M). They were formed during the early coalification equivalent to the oil window (Stach et al., 1982) and then filled in Jurassic pores and fractures.

Coal is not only an important gas-source rock but also an oil-source rock, which has been confirmed by the petroleum exploration practices in western Chinese basins, such as the Tuha Basin (Zhao and Cheng, 1998). Generally, these coals were deposited in a deltaic inter-bay swamp (Shao et al., 2003). The J_1k sedimentary facies were braided-river delta and shallow coastal lakes, where ferns and other herbaceous plants flourished (Vakhrameev, 1991). Undecomposed hydrogen-rich components carried by the river accumulated here. The enrichment of detrital exinite, coupled with the strong microbiolysis of peat swamps, resulted in coals with high hydrogen content, which laid a good environmental foundation for coal-derived hydrocarbons.

5.2 Asphalt-forming process

The Jurassic has an unconformable contact relationship with the Paleozoic basement and steadily developed in the Early and Middle Jurassic. Overall uplifting occurred in the Late Jurassic, which resulted in the absence of the Middle and Upper Jurassic in the Ruoqiang Sag. In the Jurassic, the paleo-temperature gradient was not high, 2.8°C/100 m (Li et al., 2005), and the J_1k source rock does not reach the Ro 0.5% with a maximum burial depth of only 1840 m in the QD1 well (Figure 9).

The Cretaceous in the Ruoqiang Sag is only a localized remnant even though it is 100 m thick in the Tadong and Tangguzibas Depression due to the uplifting in the study area and strong denudation of the pre-deposited strata in the late Cretaceous (Yang et al., 2001; Arnaud et al., 2003). During the Cretaceous, the J_1k source rock underwent continued subsidence and uplifting. Its maximum burial depth of 2029 m did not meet the hydrocarbon threshold. The J_1k source rock did not mature with a paleo-temperature gradient of 2.7°C/100 m (Li et al., 2005).

The regional Paleogene exhibits weakly extensional sedimentation of sandstone and mudstone (Li, 1998), while the Himalayan movement that occurred at the end of the Paleogene resulted in a large-scale withdrawal of the lake water in the Ruoqiang Sag (Li et al., 2002), and the Paleogene near the QD1 well

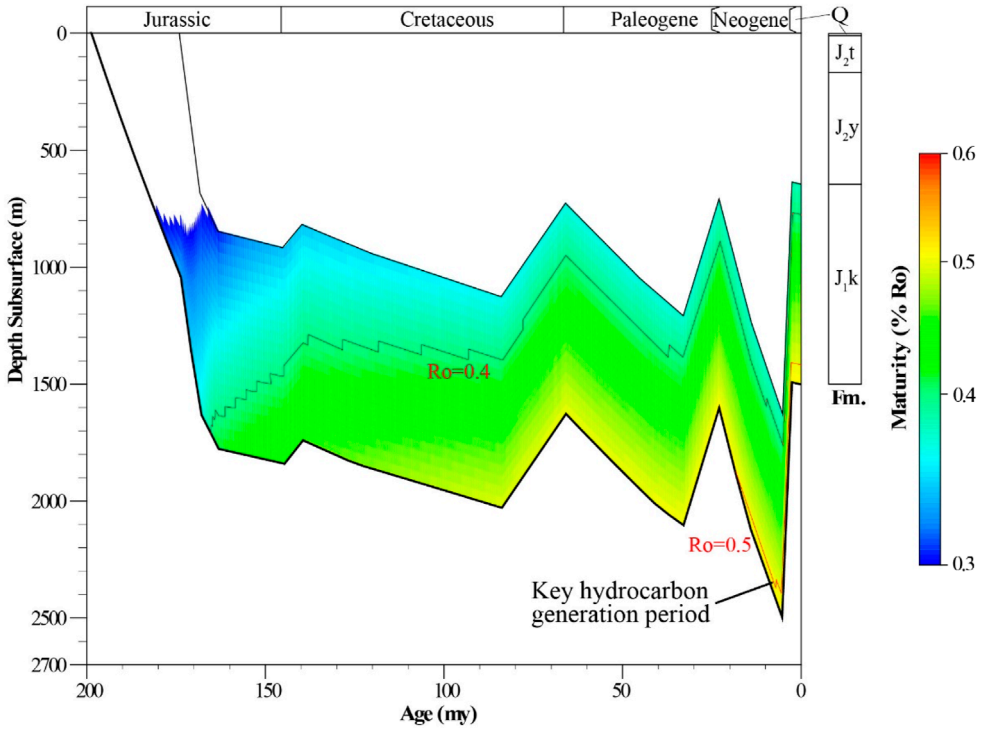

FIGURE 9
Burial and maturity evolution of the J_1k strata in the QD1 well.

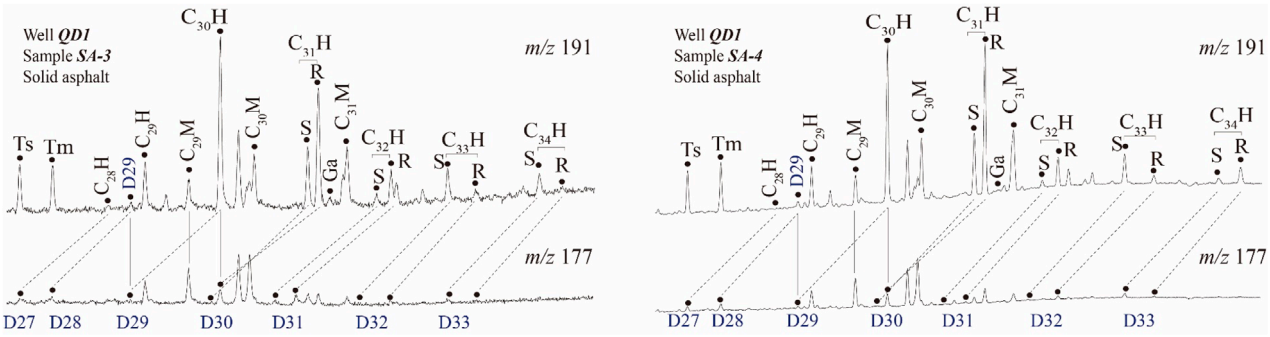

FIGURE 10
Mass chromatograms at *m/z* 191 and *m/z* 177 indicate that 25-norhopanes (indicated by a D-carbon number) occur in the Jurassic asphalt. Vertical lines indicate some peaks that yield both m/z 191 and m/z 177 ions. The C_{31}–C_{35} 17α-hopane (22S + 22R) corresponds to two C_{30}–C_{34} 25-norhopane epimers.

was also completely eroded. In the Miocene, affected by large-scale thrusting activities in the West Kunlun tectonic belt, the Ruoqiang Sag underwent flexural subsidence and deposited a thick Neogene (Tian et al., 2023). With a low paleo-temperature gradient of 2.1°C/100 m (Li et al., 2005), the J_1k burial depth met the hydrocarbon threshold with a maximum burial depth of 2500 m and Ro 0.5%, and J_1k coal began early hydrocarbon generation evolution (Figure 9). The coal macerals began the asphaltenization stage of coalification, and the exsudatinites filled in the fractures and pores, or were preserved *in situ*, or were transported to the overlying J_2y mudstone under the presence of faults, where they were accumulated, were preserved, and formed an asphalt-like appearance. After that, the Altyn Tagh Fault underwent a large-scale strike-slip activity, and the deposited Neoproterozoic was completely denuded. With the rapid rise of the Tibetan Plateau after the Pleistocene, the Quaternary was deposited only several meters thick near the QD1 well.

After the J_1k hydrocarbon evolution, the asphalt was formed from the Miocene and maintained a similar REE composition as the J_1k coal. The rhenium–osmium isotopes in the asphalt had not been sufficiently fractionated, so the ages of asphalt were consistent with the J_1k. Meanwhile, the rhenium and osmium contents indicated that they

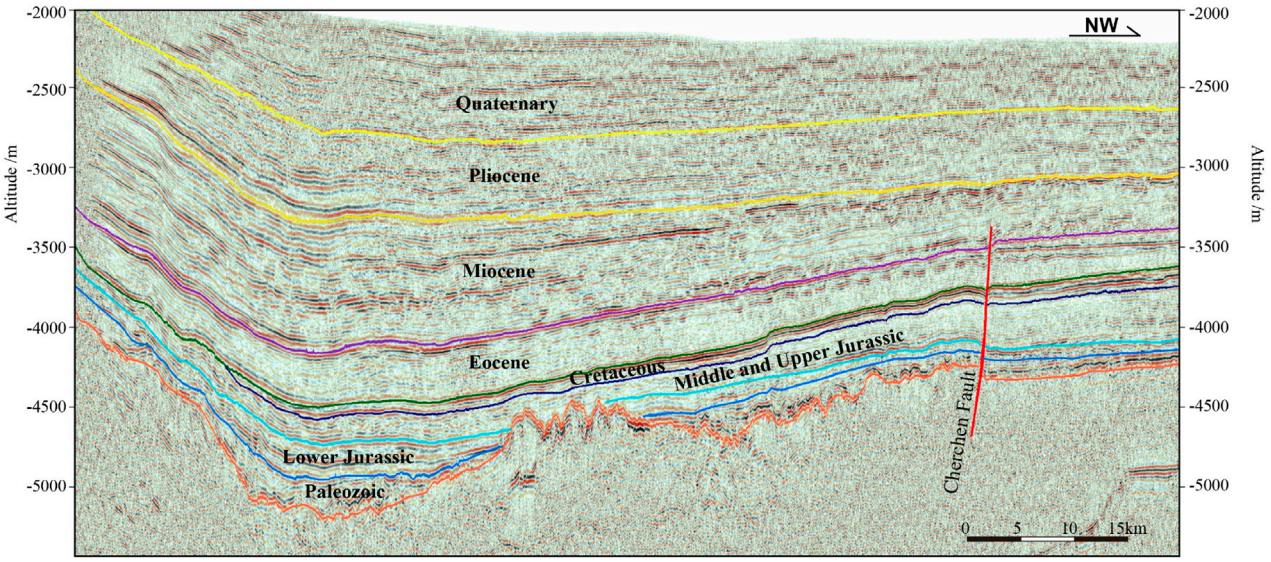

FIGURE 11
Northwest-southeast oriented seismic section of the Ruoqiang Sag. The profile is marked in Figure 1B.

came from a source rich in organic matter rather than crustal mixing during the transport process (Sun et al., 2003; Selby et al., 2007). Due to the late formation of asphalt, the 25-norbornanes were rarely detected or not detected in the *m/z* 191 composition (Figure 10). The 25-norhopanes are believed to originate from the loss of a methyl group from C-10 in hopanes and have a high abundance of biodegradation (Volkman et al., 1983). C_{29} 25-nor-17α-hopane (D29) from the C_{30} hopane has very low content of both *m/z* 191 and *m/z* 177 ions, and the ion content values of D30 and D31 from C_{31}–C_{32} 17α-hopane (22S + 22R) are only slightly higher (Figure 10). The asphalt did not undergo many secondary changes, such as oxidization and biodegradation, during its formation process.

5.3 Insights for regional petroleum exploration

Relying on samples of the QD1 well and outcrops in the Ruoqiang Sag, the Jurassic asphalt is confirmed to be derived from the J_1k coal and serves as the product of hydrocarbon generation and evolution in the early maturity of J_1k coal. The current understanding diverges considerably from the previous understanding of regional oil sources (Xu et al., 1994; Chen and Hu, 1996; Huang et al., 2013), but the current evidence is much stronger and more robust. Meanwhile, in the Tula Basin (Figure 1B), which is faulted by the Altyn Tagh Fault with Ruoqiang Sag, oil sandstones more than 100 m thick with a large amount of asphalt veins were found in the Upper Jurassic (Guo et al., 1998; Robinson et al., 2003) and were considered to be similar to the Jurassic oils in the Qaidam Basin by previous researchers, whose source rocks are also from the Middle and Lower Jurassic (Zeng et al., 2022). This undoubtedly increases the confidence in the Jurassic oil and gas exploration in the Ruoqiang Sag.

Although the understanding of the low maturity evolution degree of J_1k source rock is unfavorable for the regional Jurassic petroleum exploration, it confirms that the J_1k coal-bearing source rock has a very good hydrocarbon generation potential. Furthermore, the sampling study area is located in the premontane area at the southern margin of the Ruoqiang Sag (Figure 1). The current morphology of the Ruoqiang Sag is generally characterized by a northeast-oriented belt that is higher in the south and lower in the north (Figure 11). The Jurassic has a greater burial depth away from the premontane area and develops with a large area of J_1k and J_2y lacustrine deposits (Cheng et al., 2008; Jiang et al., 2014). From the seismic section (Figure 11), the Lower Jurassic strata are buried more than 3000 m deep and are hundreds of meters thick. Therefore, the J_1k coal-bearing source rock has matured and could provide hydrocarbons for the Ruoqiang Sag. The J_1k and J_2y have developed sedimentary facies such as deltas and shallow coastal lakes, which are favorable for the sandstone reservoirs, while the J_2y mudstone has pure lithology and large thickness and could be a very good caprock. From the analysis of the Jurassic lithological assemblage, the Ruoqiang Sag has developed a good reservoir-seal assemblage. Therefore, fault-related tectonic and lithologic traps near the hydrocarbon stove are targets for regional Jurassic petroleum exploration.

6 Conclusion

(1) According to the studies of biomarker compounds, rare earth elements, and rhenium–osmium isotopes, it is believed that the Jurassic asphalt of the QD1 well originates from the J_1k coal, which addresses the regional source rocks, responds to oil-source divergence, and confirms that the J_1k coal-bearing source rock has great hydrocarbon potential for petroleum exploration in the Ruoqiang Sag.

(2) The forming age of asphalt is determined as 192+30/−45 Ma by rhenium–osmium isotope isochrones, which is consistent

with the J_1k deposition time. The asphalt is formed late as the exsudatinite of the asphaltenization stage of coalification from the Miocene and is derived from the J_1k coal.

Data availability statement

The original contributions presented in the study are included in the article/Supplementary Material; further inquiries can be directed to the corresponding author.

Author contributions

XL: funding acquisition, methodology, and writing–original draft. ZB: investigation, resources, and writing–review and editing. YY: conceptualization, formal analysis, and writing–review and editing. ZJ: investigation, project administration, and writing–review and editing. JZ: data curation, formal analysis, and writing–review and editing.

Funding

The author(s) declare that financial support was received for the research, authorship, and/or publication of this article. The study was funded by the National Natural Science Foundation (41802169).

Acknowledgments

The authors thank Chao Li of the National Center for Geological Experimental Testing, the Chinese Academy of Geological Sciences, and Professor Dave Selby of Durham University, United Kingdom, for conducting the rhenium-osmium isotope testing work. They would also like to thank the National Natural Science Foundation (41802169) for its support of this study.

Conflict of interest

The authors declare that the research was conducted in the absence of any commercial or financial relationships that could be construed as a potential conflict of interest.

Publisher's note

All claims expressed in this article are solely those of the authors and do not necessarily represent those of their affiliated organizations, or those of the publisher, the editors, and the reviewers. Any product that may be evaluated in this article, or claim that may be made by its manufacturer, is not guaranteed or endorsed by the publisher.

References

Arnaud, N., Tapponnier, P., Roger, F., Brunel, M., Scharer, U., Chen, W., et al. (2003). Evidence for mesozoic shear along the western Kunlun and altyn-tagh fault, northern tibet (China). *J. Geophys. Res. - Sol. Ea.* 108, 1–27. doi:10.1029/2001jb000904

Boynton, W. V. (1984). "Geochemistry of the rare earth elements: meteorite studies," in *Rare earth element Geochemistry*. Editor P. Henderson (Amsterdam: Elsevier), 63–114.

Chen, R. L., and Hu, M. (1996). Discovery of jurassic oil-bearing sandstone and its oil source in the Southeast Tarim Basin. *Chin. Sci. Bull.* 41 (18), 1685–1688. doi:10.1360/csb1996-41-18-1685

Cheng, X. G., Liao, L., Chen, X. A., Guo, Q. Y., Wang, D. E., Chen, H. L., et al. (2008). Jurassic sedimentary facies and paleoenvironmental reconstruction of southeastern Tarim Basin, northwestern China. *J. China Univ. Min. Technol.* 37 (04), 519–525.

Condie, K. C. (1991). Another look at rare earth elements in shales. *Geochim. Cosmochim. Acta* 55, 2527–2531. doi:10.1016/0016-7037(91)90370-k

Creaser, R. A., Sannigrahi, P., Chacko, T., and Selby, D. (2002). Further evaluation of the Re-Os geochronometer in organic-rich sedimentary rocks: a test of hydrocarbon maturation effects in the Exshaw Formation, Western Canada Sedimentary Basin. *Geochim. Cosmochim. Acta* 66 (19), 3441–3452. doi:10.1016/s0016-7037(02)00939-0

Curiale, J. A. (1986). Origin of solid bitumens, with emphasis on biological marker results. *Org. Geochem.* 10 (1–3), 559–580. doi:10.1016/0146-6380(86)90054-9

Dembicki, H., Jr. (2009). Three common source rock evaluation errors made by geologists during prospect or play appraisals. *AAPG Bull.* 93 (3), 341–356. doi:10.1306/10230808076

Elderfield, H., and Pagett, R. (1986). Rare earth elements in ichthyoliths: variations with redox conditions and depositional environment. *Sci. Total Environ.* 49, 175–197. doi:10.1016/0048-9697(86)90239-1

Fleet, A. J. (1984). Chapter 10 - aqueous and sedimentary geochemistry of the rare earth elements. *Dev. Geochem.* 2, 343–373. doi:10.1016/B978-0-444-42148-7.50015-0

Ge, X., Shen, C. B., Selby, D., Feely, M., and Zhu, G. Y. (2020). Petroleum evolution within the Tarim Basin, northwestern China: insights from organic geochemistry, fluid inclusions, and rhenium-osmiumgeochronology of the Halahatang oil field. *AAPG Bull.* 104 (2), 329–355. doi:10.1306/05091917253

Gong, Q. L., Li, F., Lu, C. J., Wang, H. Z., and Tang, H. (2021). Tracing seawater- and terrestrial-sourced REE signatures in detritally contaminated, diagenetically altered carbonate rocks. *Chem. Geol.* 570, 120169. doi:10.1016/j.chemgeo.2021.120169

Guckert, K. D., and Mossman, D. J. (2003). Pennsylvanian coal and associated bitumen at johnson mills, shepody bay, new brunswick, Canada. *Int. J. Coal Geol.* 53 (3), 137–152. doi:10.1016/s0166-5162(02)00181-7

Guo, Z. J., Zhang, Z. C., and Zeng, F. G. (1998). Discovery of mega-thick oil sandstone and asphalt in the Jurassic System in the Tula Basin and its significance. *Chin. Sci. Bull.* 43 (22), 1898–1901. doi:10.1007/bf02883468

Hass, J. R., Shock, E. L., and Sassani, D. C. (1995). Rare earth elements in hydrothermal systems: estimates of standard partial molal thermodynamic properties of aqueous complexes of the rare earth elements at high pressures and temperatures. *Geochim. Cosmochim. Acta* 59 (21), 4329–4350. doi:10.1016/0016-7037(95)00314-p

Hendrix, M. S., Brassell, S. C., Carroll, A. R., and Graham, S. A. (1995). Sedimentology, organic geochemistry, and petroleum potential of jurassic coal measures: Tarim, junggar, and turpan basins, northwest China. *AAPG Bull.* 79 (7), 929–959. doi:10.1306/8d2b2187-171e-11d7-8645000102c1865d

Huang, Y. P., Jiang, Z. L., Luo, X., Liu, M. Y., and Duan, C. (2013). Comparison and hydrocarbon accumulation model of oil source rocks in Jianggalesayi structural belt in Tadongnan Depression of Southeastern Tarim Basin. *Xinjiang Pet. Geol.* 34 (3), 287–290.

Hwang, R. J., Teerman, S. C., and Carlson, R. M. (1998). Geochemical comparison of reservoir solid bitumens with diverse origins. *Org. Geochem.* 29 (1-3), 505–517. doi:10.1016/s0146-6380(98)00078-3

Jacob, H. (1989). Classification, structure, genesis and practical importance of natural solid oil bitumen ("migrabitumen"). *Int. J. Coal Geol.* 11 (1), 65–79. doi:10.1016/0166-5162(89)90113-4

Jiang, Z. L., Qiu, H. J., Huang, Y. P., Fu, W. K., Jiang, K. P., and Chen, J. (2014). Jurassic lacustrine source rock characteristics and its petroleum geological significance in the Southeast Depression of Tarim Basin, China. *Arab. J. Geosci.* 7, 5093–5106. doi:10.1007/s12517-013-1187-8

Li, H. B., Yang, J. S., Xu, Z. Q., Wu, C. L., Wan, Y. S., Shi, R. D., et al. (2002). Geological and chronological evidence of Indo-Chinese strike-slip movement in the Altyn Tagh fault zone. *Chin. Sci. Bull.* 47 (1), 27–32. doi:10.1360/02tb9005

Li, H. L., Qiu, N. S., Jin, Z. J., and He, Z. L. (2005). Geothermal history of Tarin basin. *Oil Gas Geol.* 26 (5), 613–617. *(in Chinese)*.

Li, W. H. (1998). Jurassic sedimentary system of fault depression in Southeast Tarim and its hydrocarbon significance. *Oil Gas Geol* 9 (2), 110–l14.

Liao, Y. H., Fang, Y. X., Wu, L. L., Cao, Q. G., and Geng, A. S. (2015). The source of highly overmature solid bitumens in the Permian coral reef paleo-reservoirs of the Nanpanjiang Depression. *Mar. Petrol. Geol.* 59, 527–534. doi:10.1016/j.marpetgeo.2014.10.008

Liu, J. J., Selby, D., Obermajer, M., and Mort, A. (2018). Rhenium–osmium geochronology and oil–source correlation of the Duvernay petroleum system, Western Canada sedimentary basin: implications for the application of the rhenium–osmium geochronometer to petroleum systems. *AAPG Bull.* 102 (08), 1627–1657. doi:10.1306/12081717105

Liu, Y. J., Genser, J., Ge, X. H., Neubauer, F., Friedl, G., Chang, L. H., et al. (2003). $^{40}Ar/^{39}Ar$ age evidence for Altyn fault tectonic activities in western China. *Chin. Sci. Bull.* 48 (18), 2024–2030. doi:10.1007/bf03183998

Mahdaoui, F., Reisberg, L., Michels, R., Hautevelle, Y., Poirier, Y., and Girard, J.-P. (2013). Effect of the progressive precipitation of petroleum asphaltenes on the Re▪Os radioisotope system. *Chem. Geol.* 358, 90–100. doi:10.1016/j.chemgeo.2013.08.038

Moldowan, J. M., Seifert, W. K., and Gallegos, E. J. (1985). Relationship between petroleum composition and depositional environment of petroleum source rocks. *AAPG Bull.* 69 (8), 1255–1268. doi:10.1306/ad462bc8-16f7-11d7-8645000102c1865d

Ritts, B. D., and Biffi, U. (2000). Magnitude of post-Middle Jurassic (Bajocian) displacement on the central Altyn Tagh fault system, northwest China. *GSA Bull.* 112 (1), 61–74. doi:10.1130/0016-7606(2000)112<61:mopjbd>2.0.co;2

Robinson, D. M., Dupont-Nivet, G., Gehrels, G. E., and Zhang, Y. Q. (2003). The Tula uplift, northwestern China: evidence for regional tectonism of the northern Tibetan Plateau during late Mesozoic–early Cenozoic time. *GSA Bull.* 115 (1), 35–47. doi:10.1130/0016-7606(2003)115<0035:ttunce>2.0.co;2

Selby, D., and Creaser, R. A. (2005). Direct radiometric dating of hydrocarbon deposits using rhenium-osmium isotopes. *Science* 308 (5726), 1293–1295. doi:10.1126/science.1111081

Selby, D., Creaser, R. A., and Fowler, M. G. (2007). Re-Os elemental and isotopic systematics in crude oils. *Geochim. Cosmochim. Acta* 71 (2), 378–386. doi:10.1016/j.gca.2006.09.005

Shao, L. Y., Zhang, P. F., Hilton, J., Gayer, R., Wang, Y. B., Zhao, C. Y., et al. (2003). Paleoenvironments and paleogeography of the Lower and lower Middle Jurassic coal measures in the Turpan-Hami oil-prone coal basin, northwestern China. *AAPG Bull.* 87 (2), 335–355. doi:10.1306/09160200936

Stach, E. M., Mackowsky, M. T., Teichmüller, M., Taylor, G. H., and Teichmüller, R. (1982). *Stach's text book of coal petrolog*. Berlin: Gebruder Borntraeger.

Sun, W. D., Bennett, V. C., Eggins, S. M., Kamenetsky, V. S., and Arculus, R. J. (2003). Enhanced mantle-tocrust rhenium transfer in undegassed arc magmas. *Nature* 422 (6929), 294–297. doi:10.1038/nature01482

Tian, H. F., Chen, H. L., Cheng, X. G., Wu, L., Lin, X. B., Gao, S. B., et al. (2023). Limited northward expansion of the Tibetan plateau in the late cenozoic: insights from the Cherchen Fault in the southeastern Tarim Basin. *Tectonics* 42 (7), e2022TC007694. doi:10.1029/2022tc007694

Tribovillard, N., Algeo, T. J., Lyons, T., and Riboulleau, A. (2006). Trace metals as paleoredox and paleoproductivity proxies: an update. *Chem. Geol.* 232 (1/2), 12–32. doi:10.1016/j.chemgeo.2006.02.012

Vakhrameev, V. A. (1991). *Jurassic and cretaceous floras and climates of the earth*. Cambridge: Cambridge University Press.

Volkman, J. K. (1986). A review of sterol markers for marine and terrigenous organic matter. *Org. Geochem.* 9 (2), 83–99. doi:10.1016/0146-6380(86)90089-6

Volkman, J. K., Alexander, R., Kagi, R. I., and Woodhouse, G. W. (1983). Demethylated hopanes in crude oils and their applications in petroleum geochemistry. *Geochim. Cosmochim. Acta* 47 (4), 785–794. doi:10.1016/0016-7037(83)90112-6

Wang, J. G., Wang, L. F., and Zhou, Q. (2000). Prospects of jurassic hydrocarbon exploration in southeast Tarim Basin. *Oil Gas Geol.* 21 (3), 259–263.

Wang, Y., Zhang, X. M., Zhang, J. F., Wang, E. C., Li, Q., and Sun, G. H. (2005). $^{40}Ar/^{39}Ar$ thermoch ronological evidence for formation and Mesozoic evolution of the northern-central segment of the Altyn Tagh fault system in the northern Tibetan plateau. *GSA Bull.* 117, 1336–1346. doi:10.1130/b25685.1

Wu, L. Y., Jin, Z. J., Liu, K. Y., Chu, Z. Y., and Yang, P. (2021). Evolution of a deeply-buried oil reservoir in the north Shuntuoguole Low Uplift, Tarim Basin, western China: insights from molecular geochemistry and Re–Os geochronology. *Mar. Petrol. Geol.* 134, 105365. doi:10.1016/j.marpetgeo.2021.105365

Xu, X., Hu, M., Zhang, Q., and Bai, S. (1994). Geochemical characteristics of the Jurassic oil-bearing sandstones in the fault depression, the SE Tarim Basin. *Exp. Pet. Geol.* 16 (4), 345–352.

Yang, J. S., Meng, F. C., Zhang, J. X., and Li, H. B. (2001). The shoshonitic volcanic rocks at hongliuxia: pulses of the Altyn Tagh Fault in cretaceous? *Sci. China* 44, 94–102. doi:10.1007/bf02911976

Yue, Y. J., Ritts, B. D., Hanson, A. D., and Graham, S. A. (2004). Sedimentary evidence against large strike-slip translation on the Northern Altyn Tagh fault, NW China. *Earth Planet. Sci. Lett.* 228 (3-4), 311–323. doi:10.1016/j.epsl.2004.10.008

Zeng, X., Wang, B., Cao, Q., Wang, A., Jia, P., Zhang, P., et al. (2022). Characteristics of Jurassic source rocks and oil and gas exploration direction in the piedmont zone between the south-western Qaidam Basin and Altun Mountain. *Geol. J.* 57 (10), 4152–4166. doi:10.1002/gj.4535

Zhao, C. Y., and Cheng, K. M. (1998). Expulsion and primary migration of the oil derived from coal. *Sci. China* 41 (04), 345–353. doi:10.1007/bf02932684